**Citation**
Cui, L. and Zhang, X. and Hao, H. 2021. Improved analysis method for structural members subjected to blast loads considering strain hardening and softening effects. Advances in Structural Engineering. 24 (12): pp. 2622-2636. http://doi.org/10.1177/13694332211007382

# Improved Analysis Method for Structural Members Subjected to Blast Loads Considering Strain Hardening and Softening Effects

Liuliang Cui, Centre for Infrastructure Monitoring and Protection, School of Civil and Mechanical Engineering, Curtin University, Kent Street, Bentley, Australia, liuliang.cui@postgrad.curtin.edu.au

Xihong Zhang*, Centre for Infrastructure Monitoring and Protection, School of Civil and Mechanical Engineering, Curtin University, Kent Street, Bentley, Australia, xihong.zhang@curtin.edu.au.

Hong Hao, Centre for Infrastructure Monitoring and Protection, School of Civil and Mechanical Engineering, Curtin University, Kent Street, Bentley, Australia, hong.hao@curtin.edu.au.

## Abstract

In analysis and design of structures subjected to blast loading, equivalent Single-Degree-of-Freedom (SDOF) method is commonly recommended in design guides. In this paper, improved analysis method based on SDOF models is proposed. Both flexural and direct shear behaviors of structures subjected to blast load are studied using equivalent SDOF systems. Methods of deriving flexural and direct shear resistance functions are introduced, of which strain hardening and softening effects are considered. To collocate with the improved SDOF models, the improved design charts accounting for strain hardening and softening are developed through systematical analysis of SDOF systems. To demonstrate the effectiveness of the proposed analysis method, a model validation is made through comparing the predictions with laboratory shock tube testing results on reinforced concrete (RC) columns. It is found that compared to the conventional approach with elastic and elastic-perfectly-plastic model, the elastic-plastic-hardening model provides more accurate predictions. Additional non-dimensional design charts considering various levels of elastic-plastic-hardening/softening resistance functions are developed to supplement those available in the design guides with elastic-perfectly-plastic resistance function only, which provide engineers with options to choose more appropriate resistance functions in design analysis.

**Keywords**: SDOF model, blast loads, flexural responses, direct shear responses, elastic-plastic-hardening/softening, design charts.

# 1 Introduction

With rapid economic development and urbanization, deliberate terrorist bombing attacks, accidental explosions, and vehicle/ship collision with structures have been more and more frequently reported. (Wikipedia, 2014; Bureau of Counterterrorism, 2017). Owing to the increasing numbers of explosion and collision events, more structures are facing the risk of being subjected to blast and impact loads in their service life, therefore need to be properly designed to resist such loads for better personnel safety and asset protections.

A large number of studies including experiments and numerical simulations have been performed to investigate structural responses subjected to blast and impact loads, as well as to develop possible mitigation technologies (Remennikov, 2003) . For example, recently Wu et al. (2009) carried out field blast tests to investigate the response of RC slabs made of ultra-high-performance fiber reinforced concrete (UHPFC) with and without fiber reinforced polymer (FRP) strengthening. Burrell et al. (2014) tested blast responses of steel fiber-reinforced concrete (SFRC) columns using shock tube facility. Although they allow direct observations of the structural performance, such experiments are in general very costly and difficult to be carried out as they require special equipment such as shock tube or testing field and researchers having competence to handle explosives. Comprehensive numerical models have also been developed and employed to simulate the dynamic response of structural elements under blast loading, which are proven yielding good predictions. For instance, Shi et al. (2008) generated a comprehensive numerical model of RC columns and derived Pressure-Impulse (P-I) diagrams. Zhang et al. (2013) modeled the blast response of laminated glass windows using a detailed 3D model with LS-DYNA, where both the dynamic material properties of glass and interlayer were considered. Tabatabaei et al. (2013) developed a finite element model and predicted the surface damage and material loss of long carbon fiber reinforced concrete panels exposed to blast loading. It is noted that reliable numerical modeling requires specialized experience and demands substantial computational resources. They are therefore often not practical for engineering design applications.

The approach of simplifying a structural element into an equivalent Single-Degree-of-Freedom (SDOF) system is predominantly used in predicting the dynamic response of structures subjected to blast loading (Li and Meng, 2002; Fallah and Louca, 2007; Carta and Stochino, 2013). Compared to experiments and numerical simulations, SDOF approach could provide reasonably close predictions of structural responses but with less cost and computational effort. Standards and design guidelines such as UFC 3-340-02 (2008) and ASCE (2010) both employ the SDOF modeling method for design analysis. It has been found that the accuracy of prediction by using SDOF method strongly depends on the reliability of the derived equivalent mass and load, and the resistance function. The current design charts and criteria given in the design guides were derived by assuming flexural governed structural response mode and elastic or elastic-perfect-plastic resistance functions. These assumptions do not necessarily represent all the possible dominant response modes and structural resistances to high-rate blast loads, therefore, may lead to inaccurate design analysis. Many researchers and engineers have commented on the possible inaccuracy of conventional SDOF method because of these oversimplification and idealization (Oswald and Bazan, 2014; Hao, 2015).

One of the shortcomings of the current design guides using SDOF method is that the structural resistance function is assumed to be either elastic or elastic-perfectly-plastic. In reality, the resistance functions of structural members vary, depending on the structural form, structural materials, and loading configurations. For example, in a study by Fallah and Louca (2007), the resistance curves of two corrugated steel walls were modeled by using FE method. One has an elastic-plastic-hardening resistance and the other has an elastic-plastic-softening resistance. Fallah and Louca setup their SDOF models using the obtained hardening and softening resistance functions from FE models, and the predicted responses were very close to FE results with a discrepancy all within 15%. They then carried out parametric study on the influence of hardening/softening index on P-I diagrams. Those observations indicated the importance in considering the hardening or softening behaviors of structures subjected to blast loads in design analysis.

In addition, most of existing SDOF analysis models mainly consider flexural response, while the shear responses are not considered (Ma et al., 2007). Under blast loading, a RC element may experience both flexural and shear failures (Menkes and Opat, 1973). When a RC member is subjected to dynamic loading with relatively low amplitude and long duration, it would develop flexural deformation and may fail due to insufficient flexural capacity; whereas, when it is subjected to a high amplitude impulsive load with short duration, direct shear failure near supports could occur (Krauthammer, 1984; Krauthammer et al., 1986) . Compared with flexural bending failure, shear failure is brittle and always associated with relatively small structural deformation which usually happens within a very short period after the blast overpressure acts on the structure element and may cause sudden collapse of structures (Low and Hao, 2002). Thus, shear failures should be carefully checked in the design of structural element subjected blast load. It is generally considered that flexural failure and shear failure normally do not occur at the same time, a structural element will enter the flexural response mode only if it manages to survive the shear response (Low and Hao, 2002). Accordingly, flexural and shear failure modes can be modelled independently (Krauthammer and Shanaa, 1990).

The primary aim of this paper is to develop an improved SDOF based analysis and design method for structural element subjected to impulsive loading. The improved method will cover both flexural response mode and shear response mode. Elastic-plastic-hardening and elastic-plastic-softening are also incorporated in the resistance functions, which will give more accurate predictions of structural response. Firstly, in Section 2 the equivalent SDOF systems for flexural and shear responses are established based on the classic structural dynamics theories (Krauthammer, 2008; Biggs, 1964). Then, in Section 3 the procedures for determining theoretical flexural and shear resistance functions are detailed. Strain rate effect is considered in the resistance function by considering the dynamic increment in material properties. The maximum displacements at midspan and supports are utilized to define the flexural and shear failure criteria, respectively. In Section 4, a working example of a RC column is presented using the above method and the predicted results are compared with the laboratory shock tube testing data. The improvement of the model is demonstrated by comparing the predictions using conventional SDOF method with elastic and elastic-perfectly-plastic resistance functions. Last but not the least, a series of non-dimensional design charts, of which the resistance functions have different levels of hardening and softening indexes, are derived as supplements to those provided in UFC 3-340-02 for use in design analysis.

## 2 Equivalent SDOF Systems

Figure 1 illustrates the flow chart of the SDOF approach for analyzing structural responses subjected to impulsive loads. The direct shear resistance capacity of the element is firstly estimated based on the preliminary design configuration and design load. Then, the shear response of the equivalent SDOF model derived with the shear deformation shape function is calculated. If the structural element survives, the flexural response will then be analyzed with another equivalent SDOF model derived with flexural deformation shape function for this element. The following section will introduce the flexural SDOF model and the shear SDOF model.

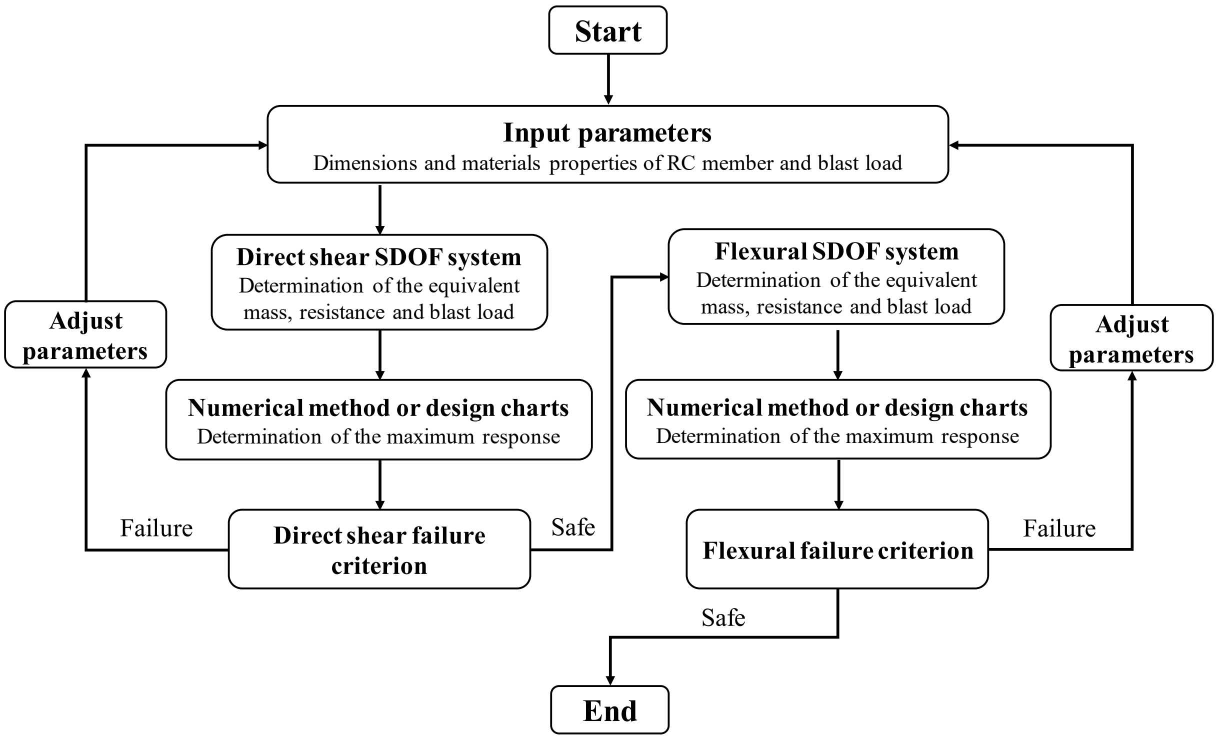


Figure 1. Flow chart of the SDOF approach to predict structural responses subjected to blast and impact loads.

### 2.1 Equivalent SDOF system for Flexural response

The SDOF system for modelling the flexural response of a structural element is based on the classic theory of Biggs (1964). In Figure 2 (a) a simply supported RC beam is employed for demonstration of the model without losing generality. It is subjected to a uniformly distributed load typically from a mid to far field explosion. The equivalent SDOF system for its flexural behavior is sketched in Figure 2 (b).

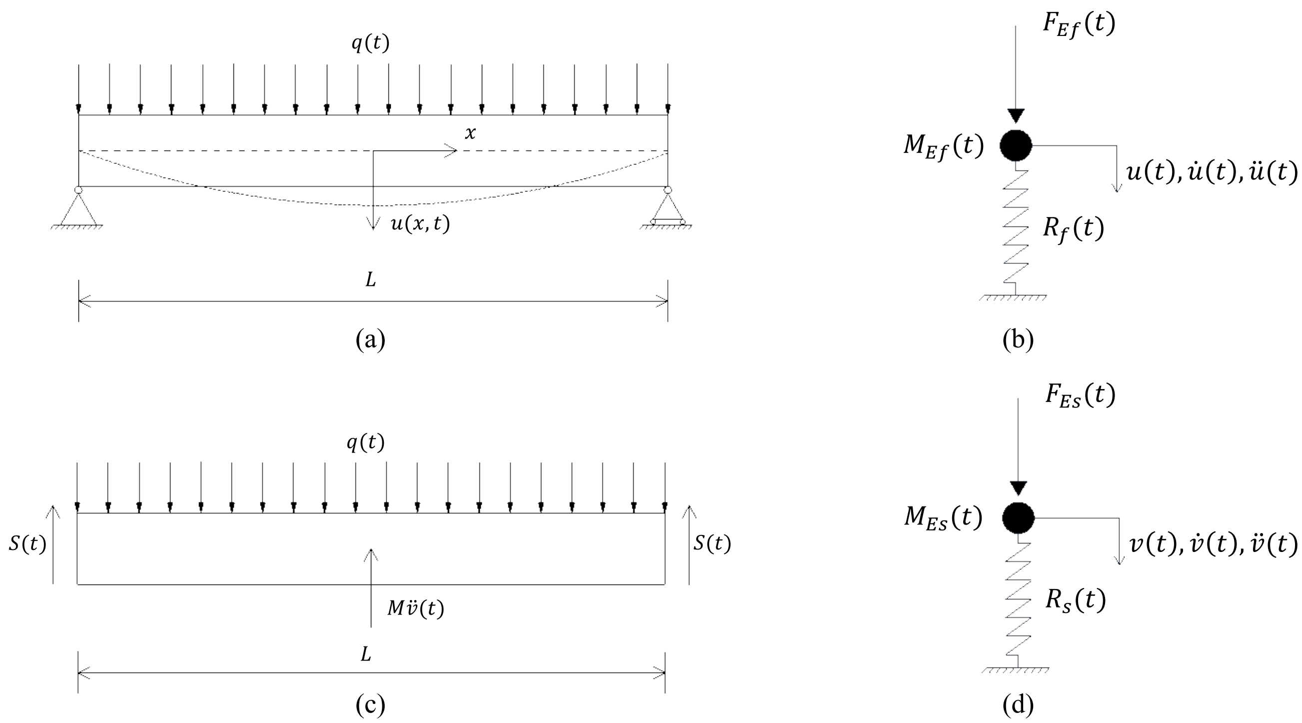


Figure 2. (a) A simply supported RC beam, (b) an equivalent flexural SDOF model of the beam, (c) dynamic force equilibrium diagram for direct shear behavior of a RC beam, and (d) an equivalent SDOF model for direct shear response of the beam.

The motion of the equivalent SDOF system can be described by the following equation

$$M_{Ef}\ddot{u}(t) + R_f(t) = F_{Ef}(t) \tag{1}$$

where $\ddot{u}$ is the acceleration at the mid-span; $M_{Ef}$, $R_f(t)$, $F_{Ef}(t)$ are the equivalent mass, resistant force and equivalent load from blast wave, respectively. Damping is neglected since only the first peak displacement matters, and damping has little effect in the first cycle of response. Following Biggs (1964), equation (1) can be rewritten as

$$K_M M\ddot{u}(t) + K_L R(t) = K_L A P_r(t) \quad or \quad K_{LM} M\ddot{u}(t) + R(t) = AP_r(t) \tag{2}$$

where $K_M$, $K_L$ and $K_{LM} = K_M / K_L$ are mass, load and load-mass transformation factors, respectively; $M$ = total mass of the system; $R(t)$=flexural resistance function of the element; $A$ =area loaded by the blast pressure; and $P_r(t)$ = time-varying blast pressure, $A \cdot P_r(t) = L \cdot q(t)$. The detailed derivations of these transformation factors for different boundary conditions can be found in Biggs (1964), which are therefore not given here for brevity.

### 2.2 Equivalent SDOF system for shear response

Commonly used design guides such as UFC 3-340-02 (2008) does not provide any method for calculating the shear mode governed response of a structural element but only the procedures for shear reinforcement design. To more accurately analyze the shear response, another SDOF model for direct shear behavior is generated. Without considering damping, the direct shear response can be described by the following equation:

$$M_{Es}\ddot{v}(t) + R_s(t) = F_{Es}(t) \tag{3}$$

where $\ddot{v}$ is the acceleration of the shear slip at the supports; $M_{Es}$, $R_s(t)$, $F_{Es}(t)$ are the equivalent direct shear mass, equivalent shear resistance and equivalent external load for direct shear, respectively. Because the direct shear failure mode is expected to occur within a very short duration upon the action of the blast load, the structure would not have any significant deformation at that time. Since the failure plane is very close to the support, the phenomenon is thus like a sudden collapse of the entire beam. Hence, the shape function for direct shear failure mode can be taken as unity as suggested by other researchers (Krauthammer et al., 1986; Low and Hao, 2002; Xu et al., 2014). The dynamic force equilibrium diagram for direct shear behavior is illustrated in Figure 2 (c) and the equivalent direct shear model is shown in Figure 2 (d). Because of symmetry, considering only one half of the element, then $M_{Es} = M/2$, $M$ is the total mass of the element; $R_s(t) = S(t)$, where $S(t)$ is the direct shear resistance at support which will be further explained in the next section, and $F_{Es}(t) = L \cdot q(t)/2 = A \cdot P_r(t)/2$. Equation (3) can be then rewritten as

$$0.5M\ddot{v}(t) + S(t) = 0.5AP_r(t) \tag{4}$$

By solving this dynamic equilibrium equation numerically, the shear slip at supports can be obtained and used for assessing the potential of direct shear failure of the beam.

# 3 Determination of Analysis Parameters and Failure Criteria

To enable the analysis using the above derived SDOF systems, the model parameters need to be determined which are detailed in this section. The derivation of the flexural resistance function, as well as the shear resistance function are provided. Strain rate effect is also taken into consideration. The failure criteria of the structural element are also presented and discussed in this section.

## 3.1 Flexural resistance function

The flexural resistance of a SDOF system is obtained by first determining the moment-curvature relation of the section. Then, by considering the support and loading conditions, the resistance-deflection relationship of the structure can be derived from the onset of loading to failure. Normally, the resultant static elastic-plastic behavior of the flexural SDOF system can be represented by a bilinear load-displacement diagram, as shown in Figure 3. The reason of constructing a bilinear resistance function is for easy use of the design charts which will be illustrated in Chapter 5. The abscissa $x$ represents deformation and the ordinate $r$ represents resistance. The dashed lines are the original resistance curves which could be obtained from the theoretical derivation, finite element analysis or experimental tests. In Figure 3, $K_e$ is the stiffness of the elastic part, and the point $(X_E, r_y)$ is the elastic limit which for RC structures is usually related to the point of reinforcement steel yielding. $K_p$ is the stiffness of the plastic part, and $X_u$ is the anticipated ultimate deformation for the structural element. If $K_p > 0$, it is an elastic-plastic-hardening model, and if $K_p < 0$, it is an elastic-plastic-softening model. The hardening/softening index (H/S index) is defined as $K_p / K_e$. The dynamic flexural resistance functions are obtained by directly using the dynamic strength of materials estimated with a constant strain rate. For the following contents of this section, a theoretical approach to derive the flexural bilinear resistance will be introduced.

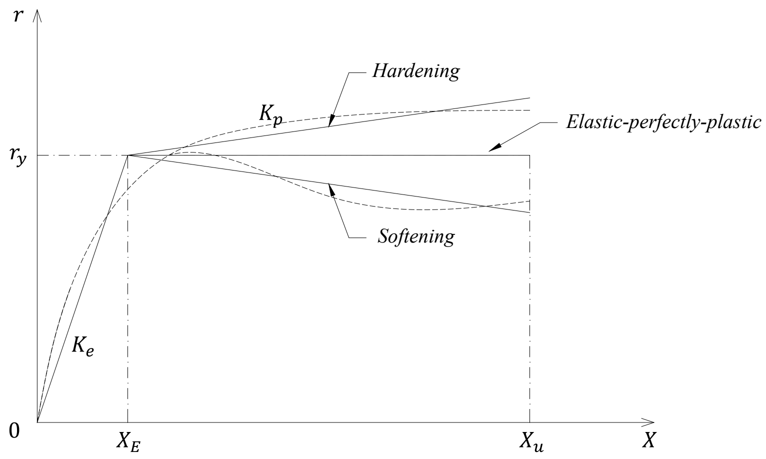


Figure 3. Idealized bilinear representation of elastic-plastic hardening and softening resistance function (the dashed lines represent the original resistance curves).

The moment-curvature relation can be obtained through layered analysis of cross-section. Taking a doubly reinforced RC element as an example, Figure 4 (a~c) shows the layered cross section and its stress and strain diagram of this element. It can be seen that the cross-section is sliced into numerous layers, and within each layer the stress and strain are assumed to be constant. Also note that this analysis considers the effects of axial load.

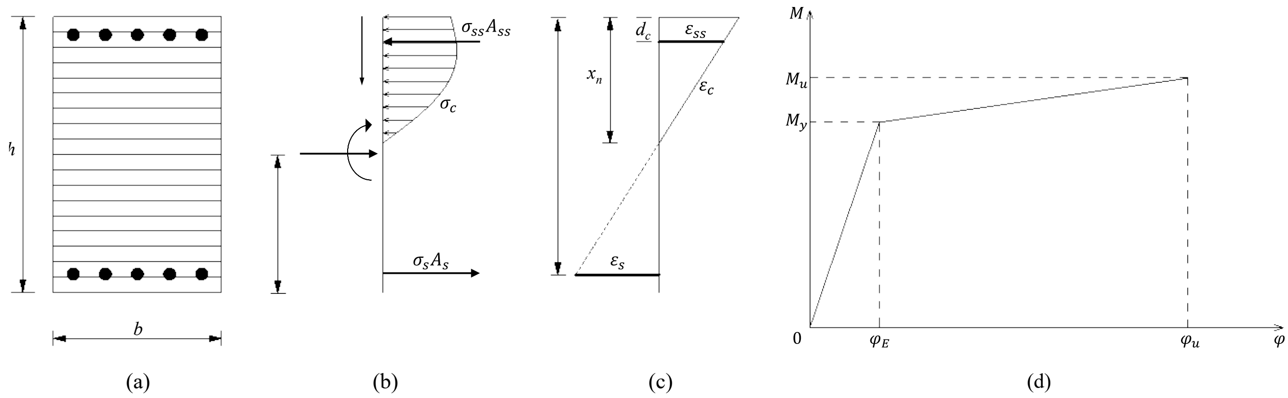


Figure 4. (a) Layered cross section of a doubly reinforced RC element; (b) stress diagram of cross section; (c) strain diagram of cross section; (d) bilinear bending moment–curvature diagram.

Given the assumptions that the cross sections of the element remain plane after deformation and that tensile resistance of concrete is neglected, the following force equilibrium equation of cross section can be derived:

$$N + \sigma_s A_s - \sigma_{ss} A_{ss} - \sum_{i=1}^{i=n} \sigma_{ci} A_{ci} = 0 \tag{5}$$

where $N$ is the axial force at the cross-section; $\sigma_s$ and $\sigma_{ss}$ are the steel stresses in the tension and compression zones; $A_s$ and $A_{ss}$ are the areas of reinforcements in tension and compression, respectively; $n$ is the number of concrete layers in compression; $\sigma_{ci}$ is the compressive stress of the $i$ th layer of concrete; $A_{ci}$ is the area of the $i$ th layer of concrete, and $A_{ci} = bx_n / n$, of which $b$ is the width of cross section and $x_n$ is the depth of the neutral axis.

Taking moment equilibrium about the neutral axis, the resultant moment $M_R$ can be calculated by

$$M_R = \sigma_{ss} A_{ss} (\frac{h}{2} - d_c) + \sigma_s A_s (h_0 - \frac{h}{2}) + \sum_{i=1}^{i=n} \sigma_{ci} A_{ci} y_{ci} \tag{6}$$

where $h$ is the depth of the cross section; $d_c$ is the depth of the concrete cover; $h_0$ is the effective depth; and $y_{ci}$ is the distance from the $i$ th layer of concrete to the neutral axis. The corresponding curvature $\varphi$ is computed by

$$\varphi = \frac{\varepsilon_s}{h_0 - x_n} \tag{7}$$

where $\varepsilon_s$ is the strain of the tension steel. Because the anticipated resistance has bilinear form, only the moment and curvature at yielding ($M_y$ and $\varphi_y$) and ultimate state ($M_u$ and $\varphi_u$) are required. The procedure for obtaining the moment-curvature relationship of the structural element can be summarized as follows:

(1) For the yielding state, $\varepsilon_s = \varepsilon_{sy}$, and for the ultimate state, $\varepsilon_{ct} = \varepsilon_{cu}$, where $\varepsilon_{sy}$ is the yielding strain of tensile steel, $\varepsilon_{ct}$ is the concrete strain of the top layer, $\varepsilon_{cu}$ is the ultimate strain of concrete which is usually assumed as 0.0038;

(2) Assume a value for the depth of the neutral axis $x_n$ at each state;

(3) Calculate $\sigma_s$, $\sigma_{ss}$, and $\sigma_{ci}$, and substitute them into Eq. (5) to check if the equilibrium is satisfied. If equilibrium is not satisfied, go back to step (2), assume a new value of $x_n$, and re-analyze step (3); if equilibrium is satisfied, go to step (4).

(4) Calculate moment ($M_y$ and $M_u$) and curvature ($\varphi_y$ and $\varphi_u$) using Eq. (6) and (7).

The method of bi-section can be used to determine the value for the depth of the neutral axis $x_n$ in step (2).

After the determination of $M_y$, $\varphi_y$, $M_u$ and $\varphi_u$, the bilinear bending moment–curvature diagram can be defined as Figure 4 (d). In this analysis, the concrete reaching the strain of $\varepsilon_{cu}$ does not represent the failure of element as redistribution of compressive force will happen. The nominal ultimate state mentioned in this section is only for the calculation of hardening/softening index. The resistance-deflection relationship can be derived as described below.

The resistance $r$ can be computed from the bending moment by considering the moment equilibrium of the element. The determination of deflection should be divided into two stages, namely elastic stage and plastic stage. Taking a simply supported beam under uniformly distributed load as an example, the resistance at yielding and ultimate state are calculated by

$$r_y = \frac{8M_y}{L} \text{ and } r_u = \frac{8M_u}{L} \tag{8}$$

where $L$ is the beam length. The deflection at midspan at yielding can be calculated from the well-known formula provided by the linear elastic theory of beams:

$$u^y_{midspan} = \frac{5L^2}{48}\varphi^y_{midspan} \tag{9}$$

The displacement in the plastic stage is evaluated by assuming that a concentrated plastic hinge is formed at the mid-span section of the beam. Here, $\theta_P$ indicates the plastic rotation at any time after the formation of plastic hinge. By introducing a fixed plastic hinge length $L_P$, and by denoting the plastic curvature as $\varphi^{P}_{midspan}$ ($\varphi^{P}_{midspan} = \varphi^{u}_{midspan} - \varphi^{y}_{midspan}$), which is assumed to be a constant over $L_p$, the total displacement at the ultimate state can be derived as

$$u^{u}_{midspan} = u^{y}_{midspan} + \frac{1}{4}(\varphi^{u}_{midspan} - \varphi^{y}_{midspan}) \cdot L_P \cdot L \tag{10}$$

By using equations (8), (9), (10) and the obtained bilinear bending moment–curvature relationship, the bilinear load-deflection diagram can be determined, as illustrated in Figure 3, where $X_E = u^{y}_{midspan}$, $X_u = u^{u}_{midspan}$, $K_e = \frac{r_y}{u^{y}_{midspan}}$, $K_p = \frac{r_u - r_y}{u^{u}_{midspan} - u^{y}_{midspan}}$.

Many approximate expressions for $L_p$ are available in literature. Here, the simple formula adopted by Carta and Stochino (2013) is used as

$$L_p = h_0 + 0.05L \tag{11}$$

The constitutive properties of concrete adopt the idealized stress-strain curve for concrete under uniaxial compression proposed by Hognestad (1951). The ascending branch of the stress-strain relationship, when $0 \le \varepsilon_c \le \varepsilon_0$, is described by the following equation:

$$\sigma_c = f_c\left[\frac{2\varepsilon_c}{\varepsilon_0} - \left(\frac{\varepsilon_c}{\varepsilon_0}\right)^2\right] \tag{12}$$

where $f_c$ is the unconfined static compressive strength of concrete, and $\varepsilon_0$ is the corresponding strain at peak compressive stress. The descending branch, when $\varepsilon_c > \varepsilon_0$, is represented by a straight line connecting the peak strength to $0.85 f_c$ at a strain of $\varepsilon_{cu}$. In the meantime, the uniaxial behavior of reinforcing steel (both in tension and in compression) is approximated to be elastic-perfectly plastic.

It is worth mentioning that in UFC 3-340-02, the influence of axial compression on moment capacity of beam elements is neglected in order to attain a more conservative design. Unfortunately, such simplifications may cause significant errors in predicting members' blast response. The comparisons with UFC's method will be presented in Chapter 4.

### 3.2 Direct shear resistance function

The direct shear resistance function of RC structures is not well developed and thus is more empirical. Figure 5 shows the resistance-slip model employed here, which was first proposed by Krauthammer et al. (1986). It is composed of five straight line segments, namely the elastic response segment OA, hardening segment AB, plastic flow segment BC, softening segment CD and final yielding segment DE. The elastic segment (segment OA) finishes at the slip of 0.1mm, and the corresponding shear stress $\tau_e$ (MPa) is given by the expression

$$\tau_e = \frac{165 + 0.157(145 f_c)}{145} \le \frac{\tau_m}{2} \tag{13}$$

where $f_c$ (MPa) is the concrete uniaxial compressive strength, and $\tau_m$ (MPa) is the maximum shear stress corresponding to the starting point of plastic flow segment (segment BC) with a shear slip of 0.3mm. $\tau_m$ is given by the expression as

$$\tau_m = \frac{8\sqrt{145 f_c} + 0.8\rho_{vt}(145 f_y)}{145} \le 0.35 f_c \tag{14}$$

where $\rho_{vt}$ is the total reinforcement ratio of the steel crossing the shear plane. In the shear flow segment (BC), the shear stress remains constant until the shear slip reaches 0.6mm. Then, the shear stress decreases as the shear slip increases. In practical application, a trilinear model is used to simplify the shear resistance curve (Krauthammer et al., 1993). In this paper, the trilinear model is further simplified into a bilinear model following Low and Hao (2002), as shown in Figure 5. The simplification is based on the energy equivalency principle that the area under the resistance-displacement curve remains constant, so that the blast energy absorbed by the system would be the same, and thus the displacement calculated would be the same as well. The yielding and the maximum allowable shear slips are taken as 0.1 mm and 0.6 mm, respectively (Low and Hao, 2002). The shear stress $\tau_y$ at point F is found to be equal to $0.5(\tau_e + \tau_m)$. Apparently, the resulted bilinear direct shear resistance function is an elastic-plastic-hardening model.

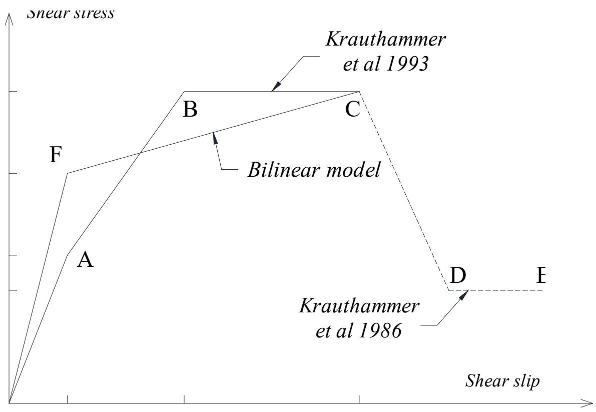


Figure 4. Direct shear resistance model

For direct shear, cracks are usually near the supports. Thus, the shape function is assumed as unity in deriving the equivalent SDOF model as discussed in section 2.2. Since the rotation at support is neglected in calculating the shear responses, the influence of different boundary conditions on this direct shear resistance model is neglected.

### 3.3 Strain rate effects

It is commonly known that the constitutive properties of concrete and steel are both strain rate sensitive. The dynamic strength will be amplified under dynamic loading comparing to those under quasi-static load.

UFC 3-340-02 (2008) has provided the recommended DIFs of concrete and reinforcing steel for design of structural members subjected to blast loading. For instance, for far field blast load, a DIF of 1.17 is suggested for reinforcing bar under bending and 1.19 for concrete. For more brittle direct shear failure a DIF of 1.1 is recommended for both concrete and reinforcing bar. In this study, those DIFs provided by UFC will be adopted. Further study will be carried out to investigate the influences of using different DIFs and different consideration methods of DIF on structural response predictions.

### 3.4 Damage criteria for flexural and direct shear failures

Based on a number of previous field blasting test and laboratory testing results on RC structures, different failure criteria have been proposed by different researchers to quantify structural damage corresponding to different failure modes (Yu and Jones, 1991; Ma et al., 2007; Huang et al., 2017). Since the maximum ductile plastic deformation is usually developed at the mid-span of a RC beam for flexural dominated response, the ratio of central deflection to half-span length is normally utilized to define the criteria for flexural bending failure; while the averaged shear strain at supports is employed to define the direct shear damage criterion since the maximum shear plastic deformation usually appears near the supports. Accordingly, based on the relevant researchers (Yu and Jones, 1991; Li and Jones, 1999; Bai and Johnson, 1982), the threshold transverse displacement due to flexural bending failure at mid-span and direct shear failure near supports can be defined as follows:

$$D_{fm} = \eta L / 2 \tag{15}$$

$$D_{sm} = \gamma_v \delta h \tag{16}$$

where $D_{fm}$ is the maximum transverse displacement at the mid-span due to flexural bending deformation; $\eta$ is the ratio of centerline deflection to half-span length; $L$ is the length of a beam; $D_{sm}$ is the maximum transverse displacement (shear slip) at supports due to direct shear deformation; $\gamma_v$ is the averaged shear strain in unit length; $\delta$ is the half-width of the shear band obtained from experimental results, and here $\delta$ is defined as 0.866 according to Li et al. (2000); and $h$ is the thickness of beam. Table 1 gives the empirical flexural bending and direct shear damage criteria for different damage levels from reference (Ma et al., 2007).

Table 1 Empirical damage criteria for bending and direct shear

| Failure mode | Criteria | Minor damage (%) | Moderate damage (%) | Severe damage (%) |
|---|---|---|---|---|
| Shear | Average shear strain | 1 | 2 | 3 |
| Bending | Ratio of centerline defection to half span | 2.5 | 6 | 12.5 |

## 4 Analysis and Model Validation

The above developed SDOF models for flexural and direct shear responses as well as the determination of their resistance functions are programmed into MATLAB. Newmark-$\beta$ method with Newton-Raphson Iteration is adopted to solve the equations of motion. The models are validated with available testing data reported by Burrell et al. (Burrell et al., 2014) on RC columns subjected to lateral impulsive loading. The SDOF model for direct shear response is firstly used to check the shear damage of the column. Then, the responses are calculated using the equivalent SDOF model based on flexural response mode. For comparison, the responses are calculated by considering the elastic-plastic-hardening resistance, as well as the elastic and elastic-perfectly-plastic resistance functions specified in UFC 3-340-02. The influences and accuracy of the idealized resistance functions on the structural response predictions are examined with respect to the testing data.

In Burrell et al.'s test program, eight RC columns were tested under impulsive loading using the shock tube at the University of Ottawa. The clear height of the columns between the supports was 1980 mm. The columns had cross-sectional dimensions of 152 mm × 152 mm and the same longitudinal reinforcement which consisted of M4–10 bars (equal tension and compression reinforcement, bar diameter=11.3 mm and reinforcement ratio=1.74%). The columns were subjected to an initial pre-compression of 294kN (about 30% of the concentric axial load capacity of the specimen). More details about the test can be found in reference (Burrell et al., 2014).

Among the tested columns, the control specimen noted as SCC-0%-75 is chosen for comparison in this study. It was constructed with plain self-consolidating concrete (SCC) with 0% steel fibers and 75mm spacing for reinforcement ties. The compressive strength of concrete was 51.6MPa, and the longitudinal reinforcement had an averaged yielding strength of 483MPa. The equivalent flexural and direct shear SDOF systems of the chosen column can be developed accordingly as Eq. (2) and Eq. (4) respectively. Since the boundary condition is considered as simply supported, $K_{LM}$ is taken as 0.78 before steel yielding and 0.66 after steel yielding for the equivalent SDOF model of the flexural response. The total mass of column $M$ is 315kg (mass of column and load-transfer device), and the loaded area $A$ is 4.129 $m^2$ (area of the shock tube opening 2.032m × 2.032m). The blast pressure is represented by a typical impulse-equivalent triangular pulse with zero rise time. The recorded peak reflected pressure and impulse in the test as input here are 87.9kPa and 780.7kPa·ms, respectively. The two equations of motion are solved using the Newmark method. Following ASCE recommendation (2010), the maximum time-step is chosen as the smaller of either one tenth of the natural vibration period of the member or one tenth of the duration of the blast.

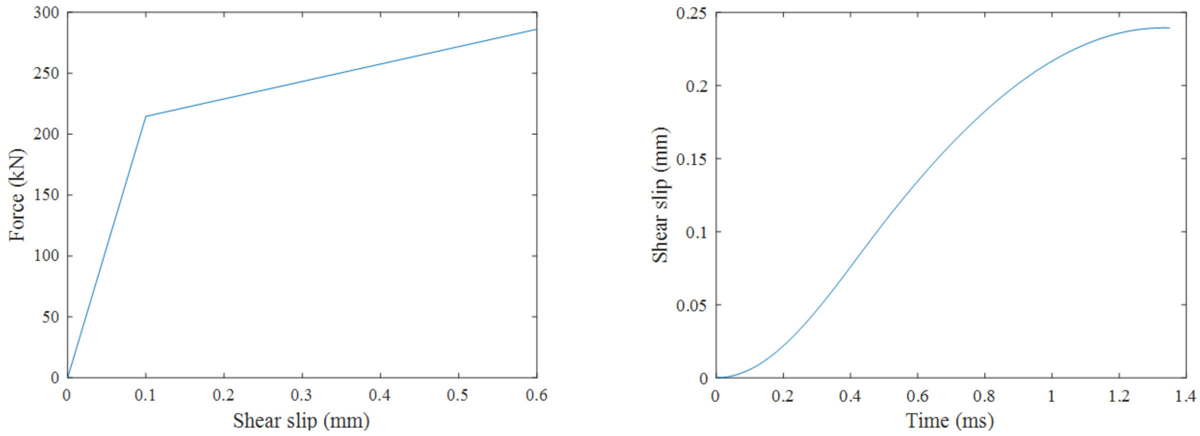


(a) (b)

Figure 5. (a) Simplified bilinear direct shear resistance function of the tested column; (b) time-histories of shear slip obtained from SDOF system.

The resistance functions used in the dynamic analysis are generated following the procedure described in section 3.1 and 3.2. Strain rate effect is taken into consideration with DIF for material dynamic strengths. For direct shear SDOF system, as suggested by UFC, a $DIF_{f_c'} = 1.1$ for concrete, and a $DIF_{f_y} = 1.1$ for the yielding strength of reinforcement are used. It is worth noting that previous researches showed increasing axial force could reduce RC member shear resistance, while some other literatures argued that under low-level axial pre-compression the shear strength of RC members could be improved (UFC, 2008; Ou and Kurniawan, 2015). UFC code recommends that under low-level axial compression, the influence on column shear capacity could be neglected. Since in this example, the level of pre-compression is relatively small, its influence on column shear resistance is therefore not considered. Figure 6 (a) shows the derived simplified bilinear direct shear resistance function of the tested column. The stiffness in elastic range (0~0.1mm shear slip) is $K_e^s = 2146\, kN/mm$, and the stiffness in plastic range (0.1~0.6mm shear slip) is $K_p^s = 143\, kN/mm$. The hardening ratio is $K_p^s / K_e^s = 0.067\,(6.7\%)$. Figure 6 (b) shows the calculated shear slip time histories near the supports. The maximum shear slip is found to be 0.24 mm, and the corresponding time is 1.35 ms. It is to be noticed that the equivalent triangular pulse has a duration of 17.8ms indicating that the direct shear response indeed occurs within a very short period before any significant deformations are developed in the RC element. Based on the direct shear damage criteria, the average shear strain $\gamma_v$ calculated using Eq. 16 is 0.18% ( $D_{sm} = \gamma_v \delta h$ , where $D_{sm} = 0.24, \delta = 0.866, h = 152$ ), which is below the minor damage threshold of 1% (as defined in Table 1). This analysis result aligns with the experimental observation that the tested column did not fail in shear damage. Since the RC element survives from direct shear responses, it will enter flexural dominated responses with relatively large deformations.

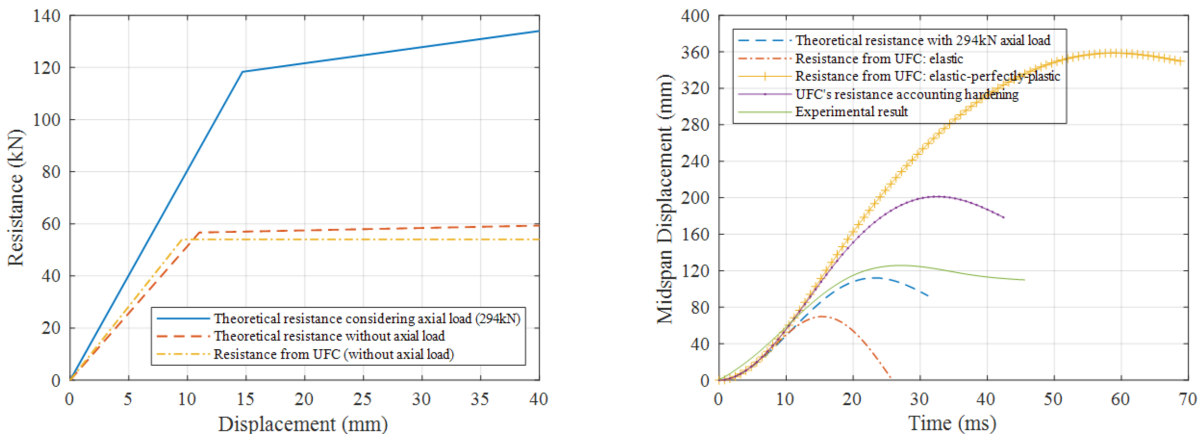


(a) (b)

Figure 6. (a) Different flexural resistance functions of the column; (b) Comparison of experimental and SDOF results

Figure 7 (a) shows the resistance curves of the column derived based on method introduced in section 3.1 and UFC's method. In this flexural SDOF system, a $DIF_{f'_c} = 1.19$ for concrete and a $DIF_{f_y} = 1.17$ for the yielding strength of reinforcement are used, as recommended in UFC. The yellow chain dotted line is the obtained resistance based on UFC's method, and the red dashed line is the theoretical resistance function without consideration of the axial load as per section 3.1. It can be observed that the UFC method gives a slightly larger initial stiffness but relatively smaller yield strength. But overall, the difference is not significant. The blue solid line denotes the theoretical resistance function with consideration of the axial pre-compression on the column. It can be seen that the axial pre-compression significantly increases the flexural resistance of the column, and apparent hardening effect can be found once yielding is reached. The equivalent elastic deflection ( $X_E$ ) is 14.7

mm, the stiffness in the elastic range ($K_e^f$) is 8.06 kN/mm and the stiffness in plastic range ($K_p^f$) is 0.62 kN/mm, thus the hardening ratio ($K_p^f / K_e^f$) is 0.077 (7.7%).

Figure 7 (b) compares the column mid-height deflection time histories between the experimental testing data with the SODF analysis using different resistance functions. Table 2 have summarized the comparison results. It can be seen that the predicted column response using the theoretical derived resistance function with consideration of axial load and hardening effect is very close to that of the test results. The maximum central deflection and the corresponding time recorded in the experiment is 126.2mm and 27.2ms, and the predicted results is 112.1 mm and 23.2 ms reflecting -11.2% and -14.7% difference. The difference could be attributed to the variation of axial load in the experiment. During the test, the axial load reduced with the shortening and rotation of the column when deformed laterally. As the axial load decreased, the moment resistance capacity of the column decreased, which led to a larger lateral deflection and longer vibration period. As expected, the SDOF model using an elastic resistance function greatly underestimates the response of the column. A maximum column central deflection of 69.8mm is predicted indicating a -45.1% difference comparing to the experimental results. This is because it largely overestimates the resistance of the column without considering column yielding. Similarly, when using the UFC recommended elastic-perfectly-plastic resistance function, the SDOF model predicts a maximum central deflection of 358.6mm, indicating a 184% higher central deflection as compared to the experimental testing results. This is mainly because the UFC method totally ignores the influence of axial pre-compression and the hardening effect, and therefore it underestimates the resistance of the column. As shown, when strain hardening effect is considered for the UFC recommended resistance function (7.7% hardening), the prediction error on the maximum deflection and time at maximum deflection could be effectively reduced to 58% and 20.6%, in comparison to 184.2% and 117.6% error by using the elastic-perfectly-plastic resistance function. The comparison demonstrates the necessity of considering the hardening effect in the resistance function, in which the improved resistance function considering hardening effect could yield much better prediction comparing to elastic only or elastic-perfectly-plastic resistance function as in the UFC design code.

Table 2 Summary of experimental and SDOF analysis results

| Results | Test | SDOF analysis with different resistance curves | | | | | | | |
|---|---|---|---|---|---|---|---|---|---|
| | | Theoretical Resistance with axial load | | Elastic | | Elastic-perfectly-plastic | | Elastic-plastic-hardening | |
| Max. deflection (mm) | 126.2 | 112.1 | Error: -11.2 % | 69.8 | Error: -45.1 % | 358.6 | Error: 184.2 % | 201.3 | Error: 58.3 % |
| Time at max. deflection (ms) | 27.2 | 23.2 | Error: -14.7% | 15.2 | Error: -44.1% | 59.2 | Error: 117.6% | 32.8 | Error: 20.6% |

# 5 Design Charts and Discussion

## 5.1 Improved design charts

The above validation demonstrates the improved SDOF analysis with consideration of hardening could give better prediction of structural response under blast loading. Although the above solution procedure is straightforward, it requires some knowledge and programming skill to solve the differential equation with nonlinear resistance function through step-by-step integration. Design guides such as UFC 3-340-02 provide charts for engineers to quickly read the maximum structural response. These design charts are plotted in the form of nondimensional curves based on systematic analysis of SDOF systems with idealized resistance functions, i.e., elastic or elastic-perfectly-plastic, for several idealized loading conditions, namely idealized triangular load or rectangular load. These design charts do not include the cases with strain-hardening or softening. Following UFC’s approach, new design charts with different levels of hardening/softening ratios of resistance curves are derived to supplement those in UFC. These generated curves would give engineers more choices in a complex circumstance and hence yield better predictions of structure responses under blast loading.

In order to utilize these response charts, both the blast loads (pressure-time history) and the resistance-deflection curve of a structural system need to be approximated. Methods for computing these idealized blast loads can refer to UFC 3-340-02 (Chapter 2) (2008), and the methods for simplification of the actual system and construct the resistance-deflection functions are presented in Section 3 of this paper.

Figure 8 and Figure 9 exhibit the generated design charts of elastic-plastic-hardening and elastic-plastic-softening SDOF systems subjected to uniformly-distributed triangular shape blast load. These design charts were obtained through MATLAB program developed in this study. Charts of the first and third columns are the maximum deflections, while charts of the second and fourth columns are the time instant corresponding to the maximum response. *P* and *T* represent the peak load and duration of the idealized blast triangular load. $X_m$ and $t_m$ are the maximum deflection and the corresponding time. From Figure 3, it is known that the resistance force of the system is defined by its elastic resistance $r_y$, elastic deflection $X_E$, and the hardening/softening index $K_p/K_e$. While $T_N$ is the natural period of the equivalent SDOF system.

Among those charts, twelve levels of hardening index, i.e. 0.005, 0.01, 0.02, 0.03, 0.04, 0.05, 0.1, 0.2, 0.3, 0.4, 0.5, 0.6, and six softening index, i.e. -0.005, -0.01, -0.02, -0.03, -0.04, -0.05 ('-' means softening), are considered which cover the likely hardening and softening behaviors of brittle concrete and ductile steel structural elements. Extrapolation of these design charts for other hardening/softening levels may not necessarily give accurate prediction. Therefore, derivation of new design charts should be carried out using the above method if needed. Since these design charts are all normalized, it is suitable for all kinds of SDOF systems once the required parameters are determined.

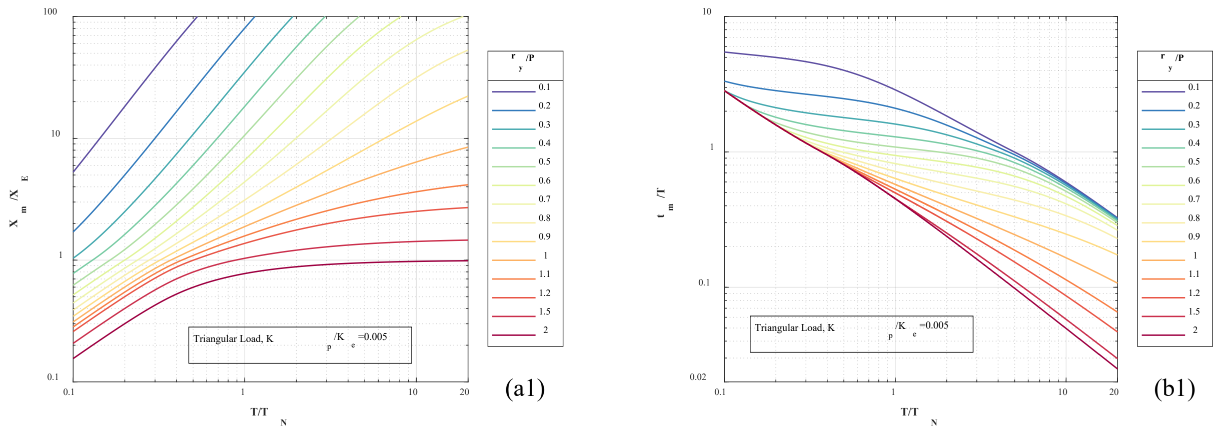

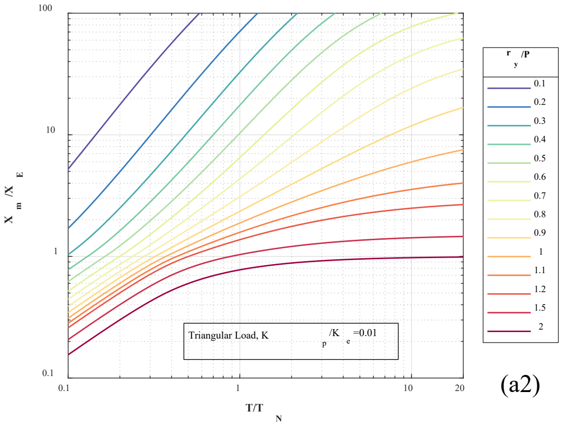


(a2)

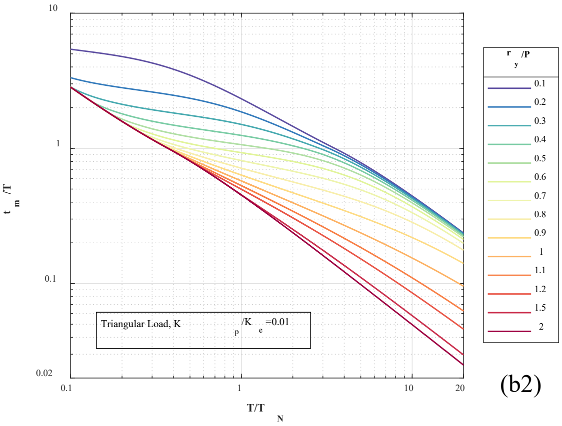


(b2)

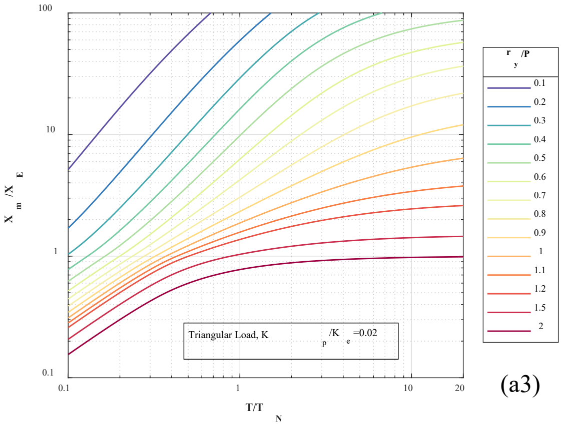


(a3)

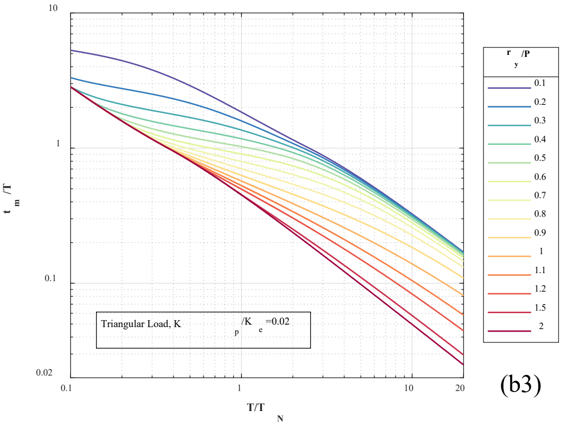


(b3)

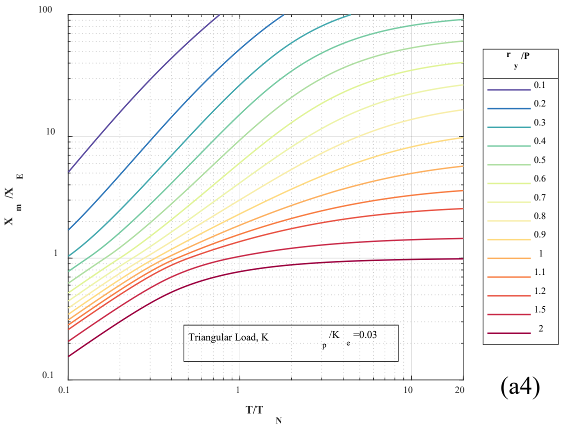


(a4)

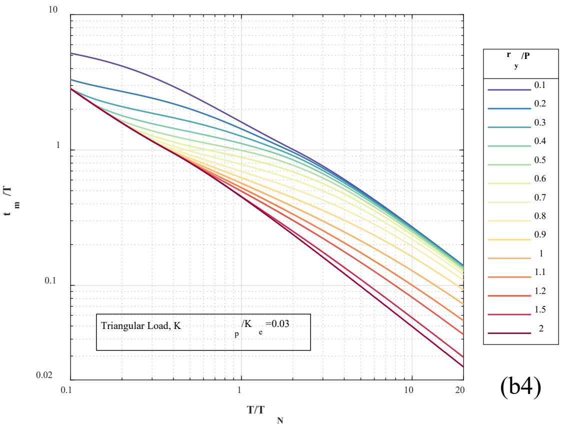


(b4)

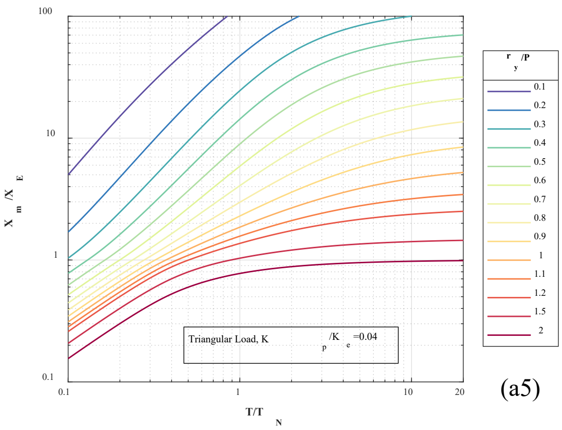


(a5)

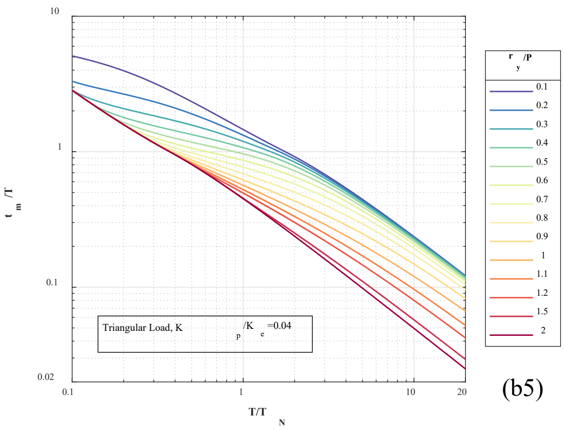


(b5)

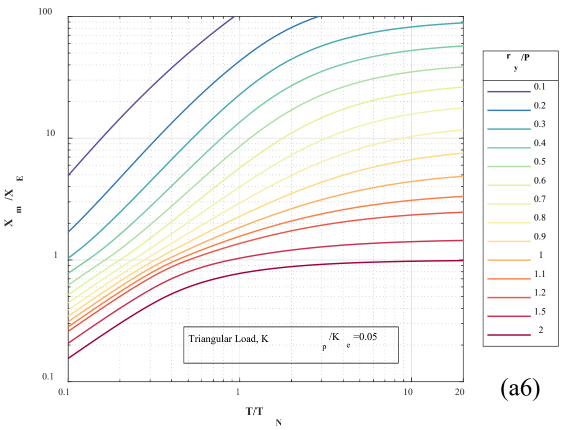


(a6)

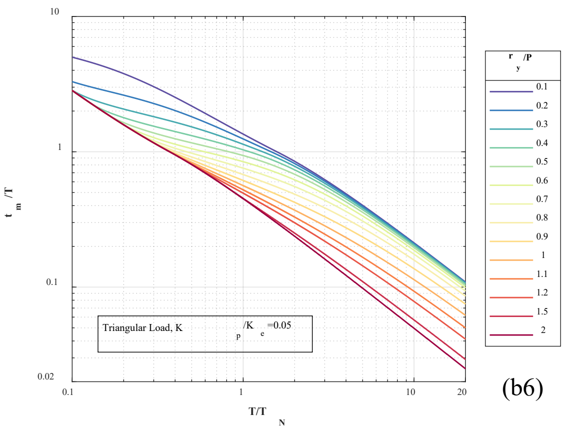


(b6)

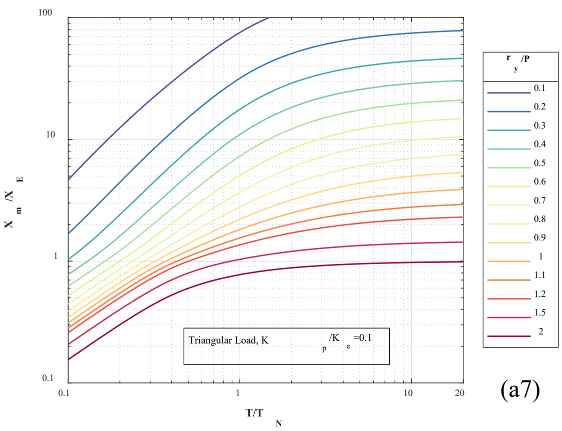


(a7)

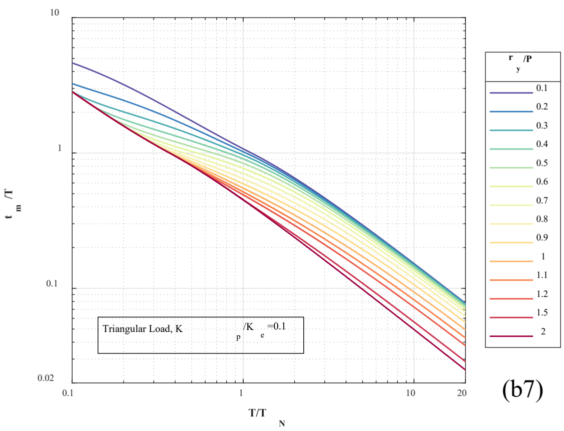


(b7)

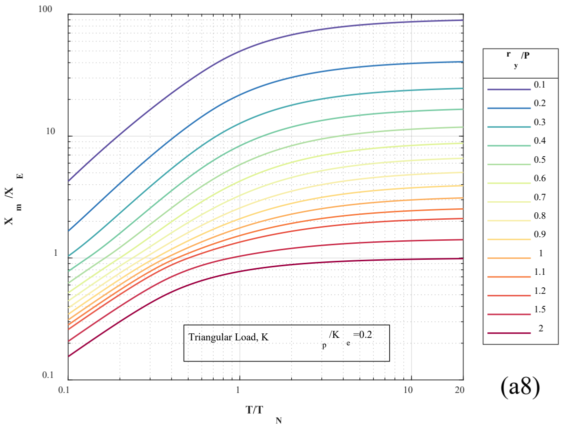

(a8)

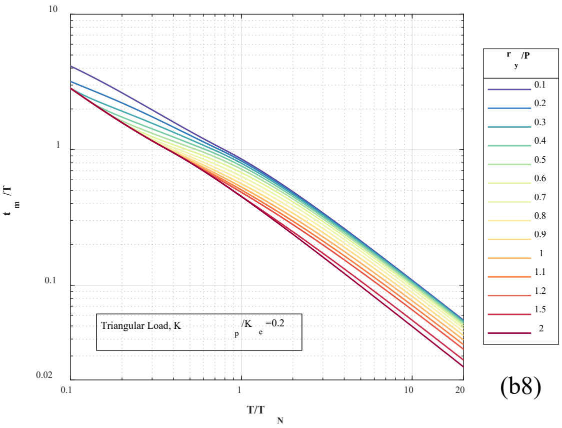

(b8)

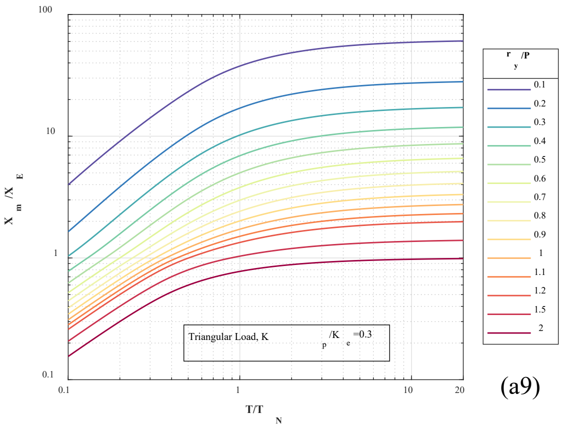

(a9)

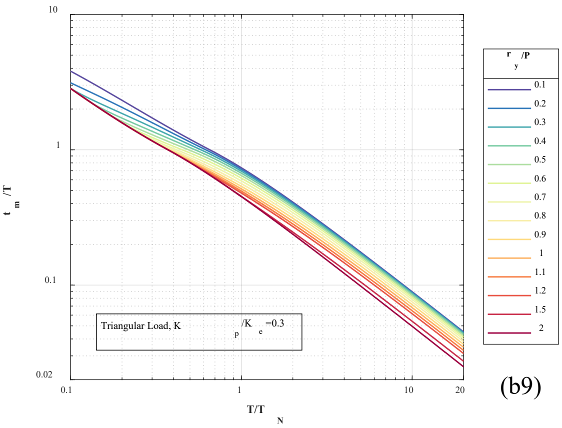

(b9)

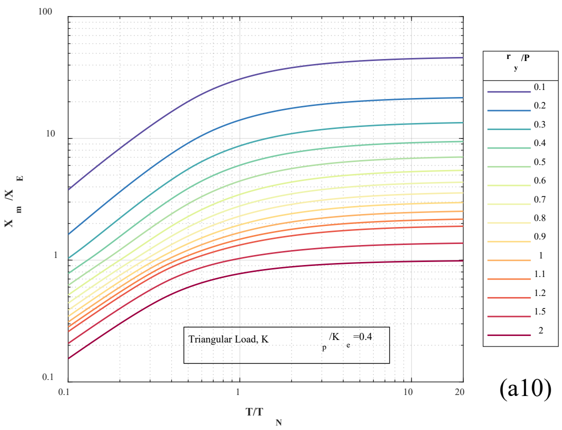

(a10)

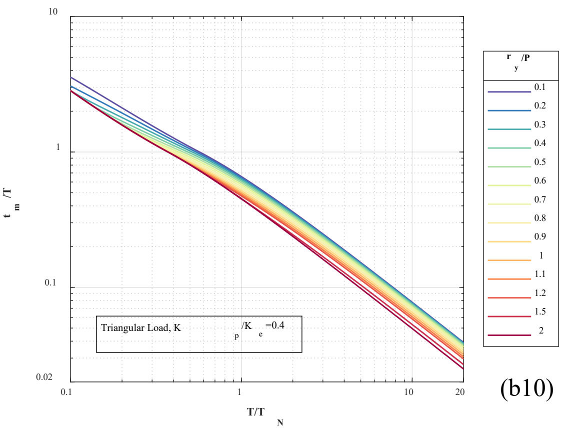

(b10)

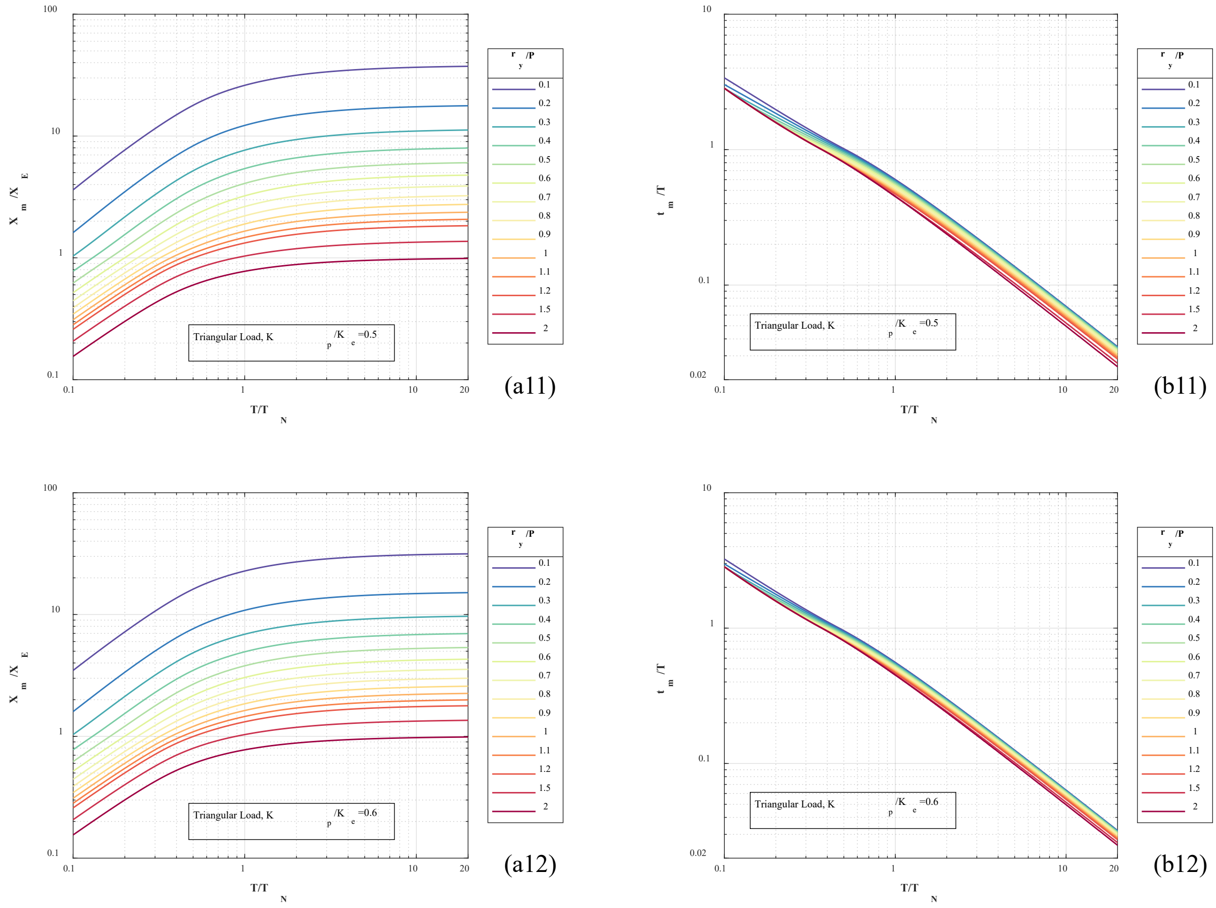


Figure 7. Design charts of elastic-plastic-hardening SDOF system for triangular load with Kp/Ke= 0.005, 0.01, 0.02, 0.03, 0.04, 0.05, 0.1, 0.2, 0.3, 0.4, 0.5, 0.6 (Maximum deflection: (a1)~(a12); Maximum response time: (b1)~(b12))

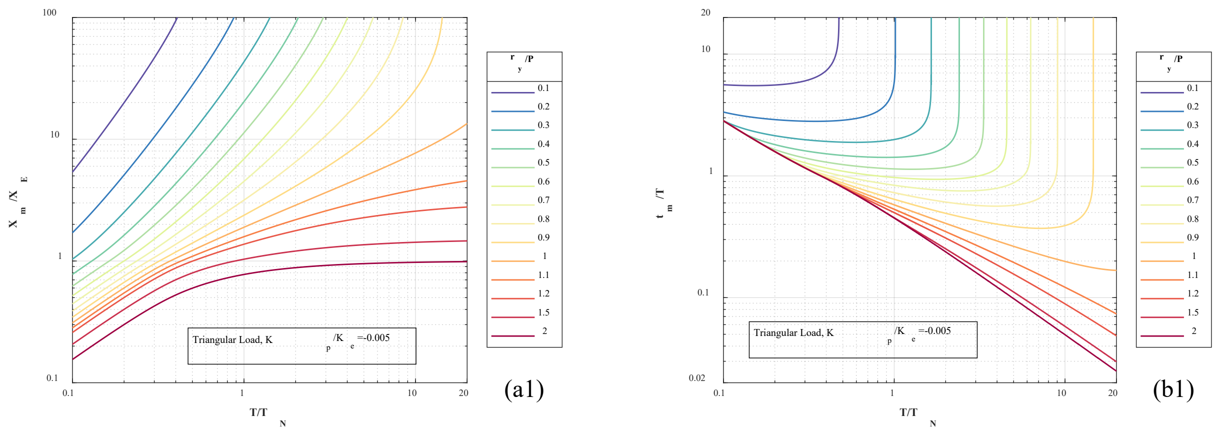

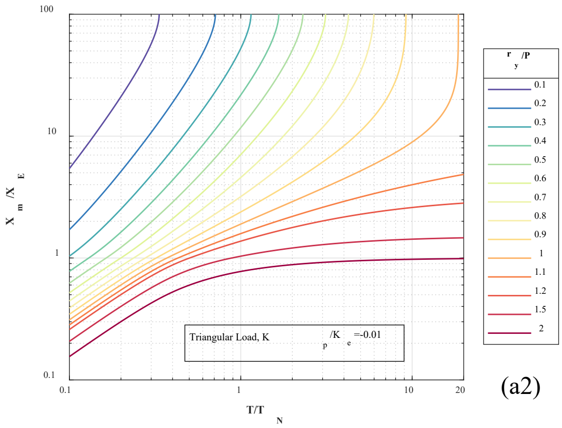


(a2)

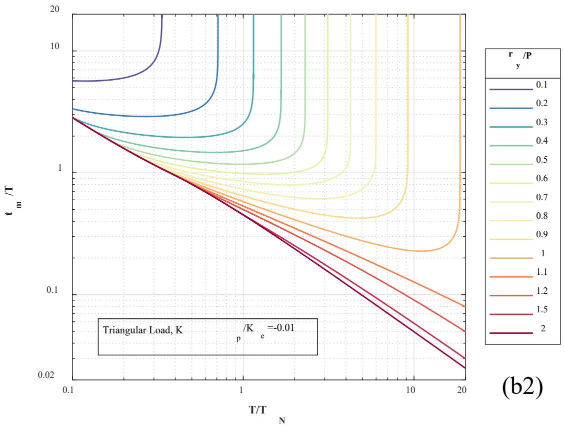


(b2)

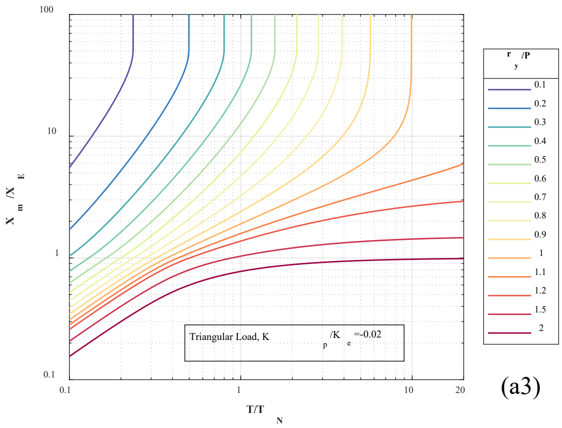


(a3)

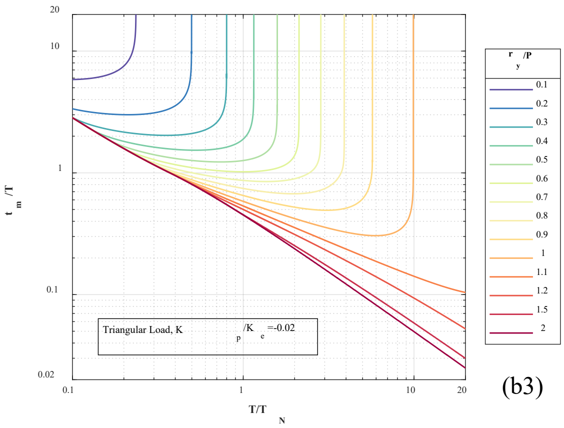


(b3)

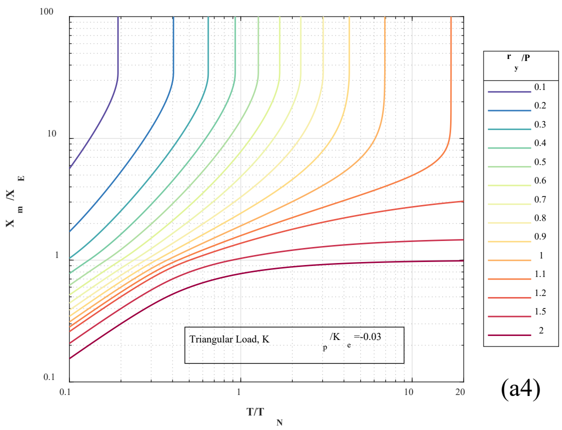


(a4)

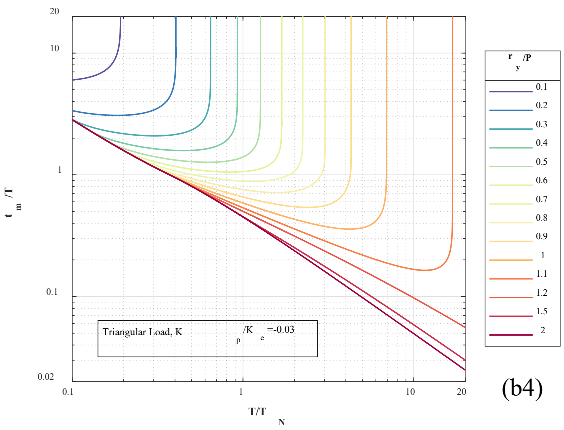


(b4)

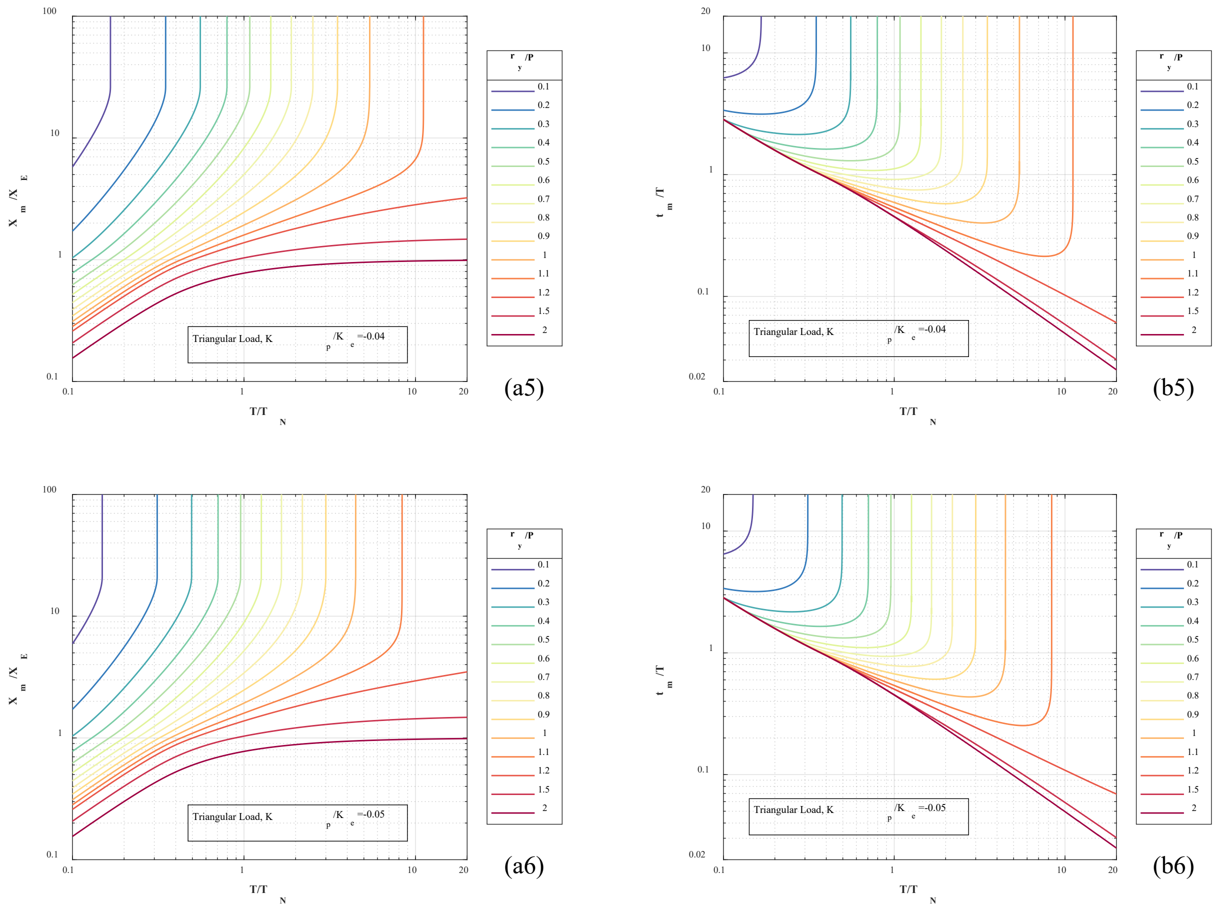


Figure 8. Design charts of elastic-plastic-softening SDOF system for triangular load with Kp/Ke= -0.005, -0.01, -0.02, -0.03, -0.04, -0.05 (Maximum deflection: (a1)~(a6); Maximum response time: (b1)~(b6))

## 5.2 Discussion

From Figure 8 (b) it can be observed that as hardening effect becomes prominent (larger hardening index value), the maximum response time $t_m/T$ curves become more and more compacted for different resistance over load ratio $r_y/P$, which indicates when there is large hardening effect, the influence of $r_y/P$ ratio becomes insignificant and negligible on structure response time ($t_m/T$). To demonstrate the structure hardening/softening effects on the maximum response of SDOF systems, the maximum deflection ($X_m/X_E$) and the maximum response time ($t_m/T$) versus loading time ($T/Tn$) relations with different hardening/softening index values are plotted for the same $r_y/P$ =0.8 in Figure 10. As shown, when $T/T_N$ is below 0.5, negligible difference can be found on the response of the structure, because only elastic response or very limited plastic response is resulted in the structure. However, as $T/T_N$ is larger than 0.5, the difference becomes more and more significant. Typically, from Figure 10 it can be easily observed that the maximum deflection reduces with the increase of the hardening ratio, and the maximum response converges to a constant value with the increase of the $T/T_N$ ratio. This is expected because as the hardening/softening index increases, the overall stiffness of the system increases as well, therefore the maximum response is smaller. The results also indicate that increasing the hardening ratio makes the structure response achieve the maximum response faster and less sensitive to the $T/T_N$ ratio. For example, when the hardening ratio is 60%, the maximum response ratio is almost stable when $T/T_N$ ratio is larger than 3.0, while the maximum response ratio still increases when $T/T_N$ ratio is 20 if the hardening ratio is 5%, implying increasing the loading duration still increases the maximum responses.

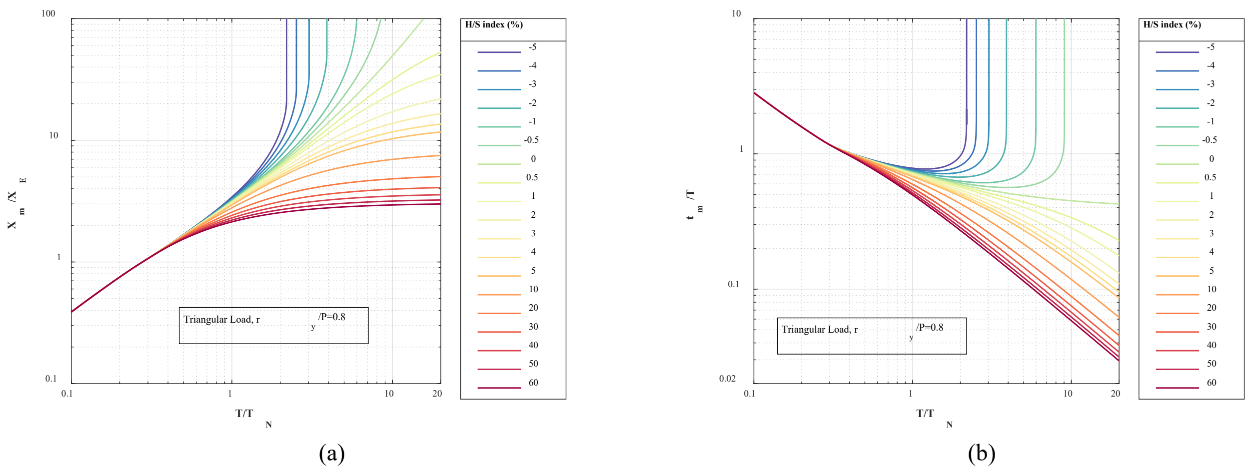


Figure 9. Illustration of the effects of the hardening/softening index on the (a) maximum deflection; and (b) corresponding response time

To further demonstrate the necessity and importance of considering hardening and softening effect, Table 3 lists the values of $X_m/X_E$ and $t_m/T$ predicted when $T/T_N$=2 and $r_y/P$ =0.8 for different H/S index as an example. The prediction errors compared with those from an elastic-perfectly-plastic system are also provided. It can be seen that even a small H/S index could cause considerable errors in structural response predictions. For instance, when a 5% hardening exists for a structure, the maximum deflection could be about 20% smaller than that predicted using conventional elastic-perfectly-plastic model; and when there is a 5% softening, the conventional elastic-perfectly-plastic model could underestimate structural maximum deflection by nearly 90%. Therefore, it is important to take hardening and softening into consideration in design analysis.

Table 3 Comparison of prediction errors for $X_m/X_E$ and $t_m/T$ with different H/S index ($r_y/P$ =0.8, $T/T_N$=2)

| H/S index | $r_y/P$ =0.8, $T/T_N$=2 | | | |
|---|---|---|---|---|
| | $X_m/X_E$ | | $t_m/T$ | |
| | Values | Errors (%) | Values | Errors (%) |
| -5% | 11.89 | 88.53 | 0.970 | 63.66 |
| -4% | 9.53 | 51.15 | 0.820 | 38.36 |
| -3% | 8.24 | 30.68 | 0.733 | 23.61 |
| -2% | 7.59 | 20.31 | 0.673 | 13.58 |
| -1% | 6.78 | 7.47 | 0.628 | 5.99 |
| -0.5% | 6.53 | 3.51 | 0.610 | 2.87 |
| 0% | 6.30 | 0.00 | 0.593 | 0.00 |
| 0.5% | 6.11 | -3.14 | 0.578 | -2.53 |
| 1% | 5.93 | -5.96 | 0.564 | -4.81 |
| 2% | 5.62 | -10.87 | 0.540 | -8.94 |
| 5% | 4.94 | -21.57 | 0.486 | -18.04 |
| 10% | 4.26 | -32.44 | 0.428 | -27.74 |
| 20% | 3.53 | -44.00 | 0.364 | -38.62 |
| 30% | 3.13 | -50.32 | 0.327 | -44.77 |
| 40% | 2.87 | -54.44 | 0.303 | -48.90 |
| 50% | 2.69 | -57.38 | 0.285 | -51.85 |
| 60% | 2.55 | -59.61 | 0.271 | -54.22 |

# 6 Conclusion

In this work, an improved analysis and design method using SDOF systems is introduced for predicting structural response under blast loading. Firstly, the direct shear response of a structural element is examined using a SDOF model corresponding to direct shear response mode. The shear resistance-slip function is derived through simplification of available 5-segment shear-slip resistance model. The shear capacity of the structure is checked. Only structure that survives the direct shear failure is further analyzed to evaluate the flexural responses. Secondly, an improved flexural SDOF model is developed by taking into consideration the strain hardening and softening as well as the axial loading effect for better prediction of structural flexural bending response. Through comparing with the conventional elastic only or elastic-perfectly-plastic resistance functions recommended in UFC, the improved model with elastic-plastic-hardening/softening resistance function gives more accurate predictions of responses of structures. Using the validated model, supplementary design charts are generated considering different levels of hardening and softening indexes for design purposes.

The generated design charts with strain hardening and softening supplement the available design charts provided by UFC 3-340-02. It is found that considering the hardening/softening structural resistance could lead to significant differences in structural response predictions as compared to the perfectly plastic assumption. For example, when the ratio of yielding resistance over peak blast load equals to 0.8 ($r_y/P$ =0.8), assuming elastic-perfectly-plastic resistance could lead to an overestimation of the maximum deflection by about 20% for a structure with 5% strain hardening and an underestimation of the maximum response by 90% for a structure with 5% strain softening. The generated design charts in this study provide engineers more choices for better predictions of the dynamic responses of structures subjected to blast load.

## Acknowledgement

The authors would like to acknowledge the financial support from Australian Research Council under ARC-Discovery Project fund DP190103253.

# References:

ASCE. (2010) Design of Blast Resistant Buildings for Petrochemical Facilities. *Task Committee on Blast Resistant Design*.

Bai Y and Johnson W. (1982) Plugging: physical understanding and energy absorption. *Metals Technology* 9: 182-190.

Biggs JM. (1964) Introduction to structural dynamics. *New York: McGraw-Hill Book Company*.

Bureau of Counterterrorism. (2017) *Country reports on Terrorism 2016*: US Department of States.

Burrell RP, Aoude H and Saatcioglu M. (2014) Response of SFRC Columns under Blast Loads. *JOURNAL OF STRUCTURAL ENGINEERING* 141: 4014209.

Carta G and Stochino F. (2013) Theoretical models to predict the flexural failure of reinforced concrete beams under blast loads. *ENGINEERING STRUCTURES* 49: 306-315.

Fallah AS and Louca LA. (2007) Pressure – impulse diagrams for elastic-plastic-hardening and softening single-degree-of-freedom models subjected to blast loading. *INTERNATIONAL JOURNAL OF IMPACT ENGINEERING* 34: 823-842.

Hao H. (2015) Predictions of structural response to dynamic loads of different loading rates. *International Journal of Protective Structures* 6: 585-605.

Hognestad E. (1951) Study of combined bending and axial load in reinforced concrete members. *University of Illinois at Urbana Champaign, College of Engineering, Experiment Station*.

Huang X, Bao H and Hao Y, et al. (2017) Damage assessment of two-way RC slab subjected to blast load using mode approximation approach. *International Journal of Structural Stability and Dynamics* 17: 1750013.

Krauthammer T. (1984) Shallow-Buried RC Box-Type Structures. *JOURNAL OF STRUCTURAL ENGINEERING* 110: 637-651.

Krauthammer T. (2008) *Modern protective structures*: CRC Press.

Krauthammer T and Shanaa H. (1990) Response of Reinforced Concrete Elements to Severe Impulsive Loads. *Journal of Structural Engineering-asce - J STRUCT ENG-ASCE* 116.

Krauthammer T, Assadi-Lamouki A and Shanaa HM. (1993) Analysis of impulsively loaded reinforced concrete structural elements—I. Theory. *COMPUTERS & STRUCTURES* 48: 851-860.

Krauthammer T, Bazeos N and Holmquist T. (1986) Modified SDOF analysis of RC box-type structures. *JOURNAL OF STRUCTURAL ENGINEERING* 112: 726-744.

Li Q and Jones N. (1999) Shear and adiabatic shear failures in an impulsively loaded fully clamped beam. *International Journal of Impact Engineering - INT J IMPACT ENG* 22: 589-607.

Li QM and Jones N. (2000) Formation of a shear localization in structural elements under transverse dynamic loads. *INTERNATIONAL JOURNAL OF SOLIDS AND STRUCTURES* 37: 6683-6704.

Li QM and Meng H. (2002) Pressure-Impulse Diagram for Blast Loads Based on Dimensional Analysis and Single-Degree-of-Freedom Model. *JOURNAL OF ENGINEERING MECHANICS* 128: 87-92.

Low HY and Hao H. (2002) Reliability analysis of direct shear and flexural failure modes of RC slabs under explosive loading. *ENGINEERING STRUCTURES* 24: 189-198.

Ma GW, Shi HJ and Shu DW. (2007) P – I diagram method for combined failure modes of rigid-plastic beams. *INTERNATIONAL JOURNAL OF IMPACT ENGINEERING* 34: 1081-1094.

Menkes S and Opat H. (1973) Broken Beams. *EXPERIMENTAL MECHANICS* 13: 480-486.

Oswald C and Bazan M. (2014) Comparison of SDOF analysis results to test data for different types of blast loaded components. In *Structures Congress 2014*, 117-130.

Ou Y and Kurniawan DP. (2015) Effect of axial compression on shear behavior of high-strength reinforced concrete columns. *ACI STRUCTURAL JOURNAL* 112: 209-219.

Remennikov AM. (2003) A review of methods for predicting bomb blast effects on buildings. *Journal of battlefield technology* 6: 5.

Shi Y, Hao H and Li Z. (2008) Numerical derivation of pressure – impulse diagrams for prediction of RC column damage to blast loads. *INTERNATIONAL JOURNAL OF IMPACT ENGINEERING* 35: 1213-1227.

Tabatabaei ZS, Volz JS and Baird J, et al. (2013) Experimental and numerical analyses of long carbon fiber reinforced concrete panels exposed to blast loading. *INTERNATIONAL JOURNAL OF IMPACT ENGINEERING* 57: 70-80.

UFC 3-340-02. (2008) Structures to resist the effects of accidental explosions. *Washington DC, Unified Facilities Criteria*.

Wikipedia. (2014) 2014 East Harlem gas explosion. Avaulable at: https://en.wikipedia.org/wiki/2014_East_Harlem_gas_explosion.

Wu C, Oehlers DJ and Rebentrost M, et al. (2009) Blast testing of ultra-high performance fibre and FRP-retrofitted concrete slabs. *ENGINEERING STRUCTURES* 31: 2060-2069.

Xu J, Wu C and Li Z. (2014) Analysis of direct shear failure mode for RC slabs under external explosive loading. *INTERNATIONAL JOURNAL OF IMPACT ENGINEERING* 69: 136-148.

Yu J and Jones N. (1991) Further experimental investigations on the failure of clamped beams under impact loads. *INTERNATIONAL JOURNAL OF SOLIDS AND STRUCTURES* 27: 1113-1137.

Zhang X, Hao H and Ma G. (2013) Parametric study of laminated glass window response to blast loads. *ENGINEERING STRUCTURES* 56: 1707-1717.